

Modern theories of low-energy astrophysical reactions

L. E. Marcucci ^a, Kenneth M. Nollett ^b, R. Schiavilla ^c, and
R. B. Wiringa ^b

^a*Department of Physics, University of Pisa, and INFN-Sezione di Pisa, I-56127 Pisa, Italy*

^b*Physics Division, Argonne National Laboratory, Argonne, Illinois 60439*

^c*Jefferson Lab, Newport News, Virginia 23606*

and Department of Physics, Old Dominion University, Norfolk, Virginia 23529

Abstract

We summarize recent *ab initio* studies of low-energy electroweak reactions of astrophysical interest, relevant for both big bang nucleosynthesis and solar neutrino production. The calculational methods include direct integration for np radiative and pp weak capture, correlated hyperspherical harmonics for reactions of $A = 3, 4$ nuclei, and variational Monte Carlo for $A = 6, 7$ nuclei. Realistic nucleon-nucleon and three-nucleon interactions and consistent current operators are used as input.

Key words: astrophysical reaction rates, radiative capture, weak capture

PACS: 21.45.+v, 25.10.+s, 26.35.+c, 26.65.+t

1 Realistic interactions and opportunities for astrophysics

Combined partial-wave analyses [1] of essentially all elastic nucleon-nucleon (NN) scattering data have been used to construct highly accurate potential models [2,3,4] that describe the NN interaction with high precision, the “realistic” interactions. Available methods allow nuclear wave functions, binding energies, and electroweak matrix elements to be computed from these potentials for nuclei containing up to ten nucleons [5,6] with great success in matching the laboratory data. All of this is done with only bare interactions between pairs or triples of nucleons, and not with the effective interactions tailored to each class of problem that are more typical of nuclear physics. In particular, simpler potential models [7,8,9,10,11] of radiative captures in light nuclei need spectroscopic factors provided by experiment, while the resonating group and similar techniques [8,12,13,14,15,16,17,18,19,20] rely on nuclear

interactions tailored to each system and use limited model spaces that affect the accuracy of cross section calculations in difficult-to-predict ways [19,20].

The mass and energy range accessible at present to calculations from realistic interactions and currents corresponds to two important areas of astrophysics: nucleosynthesis during the big bang [21] and hydrogen burning by the *pp* chain in low-mass stars including the sun [22,23]. The present paper reviews the methods and results of recent theoretical work on several rates important for these problems.

The chemical composition of the universe just after the big bang was set by the freezeout of nuclear reactions when the universe was less than about five minutes old, a process called big-bang nucleosynthesis (BBN) [21,24]. The main products are hydrogen and ^4He , in a ratio set mainly by weak interactions when the universe was about one second old. Small amounts of ^2H , ^3He and ^7Li were also made, and their abundances after BBN provide crucial information on the mean baryon density in the universe [25]. Theoretical predictions of these abundances depend on the cross sections for eleven key nuclear reactions [26], all empirically determined quantities. At present, the reactions accessible to the methods discussed here are the radiative captures $d(p, \gamma)^3\text{He}$, $p(n, \gamma)d$, $^3\text{He}(\alpha, \gamma)^7\text{Be}$, and $^3\text{H}(\alpha, \gamma)^7\text{Li}$. The first two of these are crucial for the ^2H yield of BBN, and the last three are crucial for the ^7Li yield.

The rates of energy and neutrino generation in the sun are set by the rate of the first reaction in the *pp* chain, the weak capture $p + p \rightarrow d + e^+ + \nu_e$ [22]. The cross section for this process is so small that it cannot be measured in the laboratory, so it must be provided by theory. The rates of other *pp*-chain reactions (reviewed by Haxton, Rolfs and Parker in this volume) do not appreciably affect energy generation in the Sun, but they do set the flux and energy distribution of solar neutrinos. In particular, the radiative captures $^3\text{He}(\alpha, \gamma)^7\text{Be}$ and $^7\text{Be}(p, \gamma)^8\text{B}$ are accessible in the laboratory, but the Coulomb barrier and the low (~ 20 keV) energies involved make the cross sections very small and the experiments difficult. The absolute normalization is the crucial property of a cross section for astrophysics, and this is precisely what is most difficult to measure reliably in the laboratory. A theoretical treatment must be grounded in first principles in order to provide independent information about absolute cross sections. Theoretical calculations are also possible for weak decays of ^7Be and ^8B that actually produce the neutrinos. An additional process important for the solar neutrino spectrum, the weak capture $^3\text{He} + p \rightarrow ^4\text{He} + e^+ + \nu_e$ (the “*hep*” reaction), is accessible to these methods but not at all to experiment.

2 The nuclear Hamiltonians

The Hamiltonians we use include nonrelativistic one-body kinetic energy, any of several modern, accurate two-nucleon potentials, and a three-nucleon

potential motivated by meson-exchange or chiral effective field theory:

$$H = \sum_i K_i + \sum_{i < j} v_{ij} + \sum_{i < j < k} V_{ijk} . \quad (1)$$

The kinetic energy operator is predominantly charge-independent (CI), but has a small charge-symmetry-breaking (CSB) component due to the difference between proton and neutron masses. The modern high-precision two-nucleon (NN) potentials we consider are the Argonne v_{18} (AV18) [2], CD-Bonn [3], Nijm-I, Nijm-II, and Reid93 [4]. All these potentials are charge-dependent (CD), reproducing both the pp and np scattering lengths, as well as the deuteron binding energy, and fitting a total of 4301 NN scattering data from the 1993 Nijmegen partial wave analysis (PWA93) [1] up to $E_{lab} = 350$ MeV with a $\chi^2/\text{datum} \approx 1$.

The AV18 potential is given by a sum of electromagnetic, one-pion-exchange (OPE), and short-range phenomenological terms. The strong interaction part is written as a sum of operator components:

$$v_{ij} = \sum_{p=1,18} v_p(r_{ij}) O_{ij}^p \quad (2)$$

$$O_{ij}^{p=1,8} = [1, \sigma_i \cdot \sigma_j, S_{ij}, \mathbf{L} \cdot \mathbf{S}] \otimes [1, \tau_i \cdot \tau_j] . \quad (3)$$

The first eight operators are the most important, reproducing the CI average of S- and P-wave phase shifts, while six additional terms quadratic in momentum are required to fit higher partial waves, and four small CD and CSB terms are required to explain fine differences between pp , np , and nn scattering. AV18 is local in every partial wave, and all partial waves are connected by this underlying operator structure.

All the other potentials are defined partial wave by partial wave. The Nijm-II and Reid93 potentials are local in each partial wave, while the Nijm-I central force includes momentum-dependent terms that give rise to non-local structures in configuration space. The CD-Bonn potentials have non-local components in both central and tensor parts of the interaction. All these modern potentials have about 40 parameters adjusted to fit the NN data. They cover a range of possible behaviors, as exhibited in their deuteron wave functions, shown in Fig. 1 of Ref. [27]. Despite these differences in detail, all five models give almost identical deuteron observables.

The realistic NN potentials give varying amounts of binding in the triton, ranging from 7.6 MeV for the local potentials to 8.0 MeV for the most non-local, compared to the experimental value of 8.48 MeV. In the α -particle, the binding ranges from 24.0 to 26.3 MeV, compared to the experimental 28.3 MeV [28]. Thus empirically, we need to add some three-nucleon ($3N$) potential to obtain the proper binding and size of light nuclei. On the basis of meson-exchange theory we certainly expect $3N$ potentials to play a role, while chiral perturbation theory suggests there should be a rapid convergence in the contributions of many-body forces, so we may neglect four-nucleon forces.

The $3N$ forces we use are the Tucson-Melbourne (TM) potential [29], its chirally-improved successor TM' [30], or one of the Urbana potentials [31]. These take the general form:

$$V_{ijk} = V_{ijk}^{2\pi,S} + V_{ijk}^{2\pi,P} + V_{ijk}^R . \quad (4)$$

The TM and TM' potentials are constructed from two-pion exchange, where an intermediate πN scattering takes place in either S- or P-waves. The pion-range functions embedded in these terms have a cutoff that may be adjusted to fit the triton binding energy when used in conjunction with a particular NN potential. The Urbana potentials neglect the small S-wave term, but add a phenomenological short-range repulsion, V_{ijk}^R . In this case, the pion-range functions are taken to be the same as in the NN potential, while the strength of the terms are adjusted to reproduce the binding energy of the triton and to give a reasonable saturation density in nuclear matter. Urbana model IX (UIX) [32] was adjusted specifically to go with AV18. A more sophisticated set of Illinois model $3N$ potentials has been constructed recently [5], which include an additional three-pion ring term, $V_{ijk}^{3\pi,\Delta R}$. The combined AV18/IL2 Hamiltonian reproduces light nuclear binding energies very well up to $A = 10$, but it has not yet been used in astrophysical rate calculations.

3 Transition rates

The capture processes of interest in the present study involve radiative or weak transitions between an initial two-cluster continuum state $|\mathbf{p}; J_1 M_1, J_2 M_2\rangle^{(+)}$, with clusters A_1 and A_2 having spins $J_1 M_1$ and $J_2 M_2$, respectively, and relative momentum \mathbf{p} , and a final A -nucleon bound state $|J_A M_A\rangle$. The cross section and polarization observables are obtained from matrix elements of the current operator connecting these two states. For example, the spin-averaged differential cross section for radiative capture in the center-of-mass (CM) reference frame is written as

$$\begin{aligned} \frac{d\sigma^\gamma}{d\Omega}(E, \theta) &= \frac{\alpha}{2\pi v} \frac{q}{1 + q/m_A} \\ &\times \sum_{\lambda M_A} \overline{\sum_{M_1 M_2}} |\langle -\mathbf{q}; J_A M_A | \hat{\epsilon}_\lambda^*(\mathbf{q}) \cdot \mathbf{j}^\dagger(\mathbf{q}) | p\hat{\mathbf{z}}; J_1 M_1, J_2 M_2 \rangle^{(+)}|^2 , \end{aligned} \quad (5)$$

where \mathbf{q} is the momentum of the emitted photon, $\hat{\epsilon}_\lambda(\mathbf{q})$, $\lambda = \pm 1$, are the spherical components of its polarization vector, and $\mathbf{j}(\mathbf{q})$ is the nuclear electromagnetic current operator (see Sec. 4 below). The final bound state is recoiling with momentum $-\mathbf{q}$. The $\hat{\mathbf{p}}$ -direction has been taken to define the spin quantization axis, and p depends on the relative energy $E=p^2/(2\mu)$, μ being the A_1 - A_2 reduced mass. The angle θ is the angle between $\hat{\mathbf{z}}$ and $\hat{\mathbf{q}}$, α is the fine-structure constant, m_A is the bound-state mass, $v = p/\mu$ is the relative velocity, and the photon energy q is fixed by energy conservation.

The dependence of the observables upon θ can be derived from the expansion of the initial capture state $|\mathbf{p}; J_1 M_1, J_2 M_2\rangle^{(+)}$ into partial waves $|LSJM\rangle^{(+)}$, and from the multipole expansion of the current operator [33]. The total cross section, however, is simply given by

$$\sigma^\gamma(E) = \frac{2\alpha}{v} \frac{q}{1+q/m_A} \frac{1}{(2J_1+1)(2J_2+1)} \times \sum_{l \geq 1} \sum_{LSJ} \left[|E_l(q; LSJ)|^2 + |M_l(q; LSJ)|^2 \right], \quad (6)$$

where E_l and M_l denote the reduced matrix elements of the electric and magnetic multipoles, i.e. $E_l(q; LSJ) \equiv \langle J_A || E_l(q) || LSJ \rangle^{(+)}$ and similarly for $M_l(q; LSJ)$.

The weak processes considered in the present study are proton weak capture on ^1H and ^3He , nuclear β^\pm -decay and ^7Be decay by electron (ϵ -) capture. The cross section for the proton weak capture reactions is written as

$$\sigma^\beta(E) = \int 2\pi \delta(E_i - E_f) \frac{1}{v} \sum_{ses_\nu} \overline{\sum_{M_1 M_2}} |\langle f | H_W | i \rangle|^2 \frac{d\mathbf{p}_e}{(2\pi)^3} \frac{d\mathbf{p}_\nu}{(2\pi)^3}, \quad (7)$$

where H_W is the weak-interaction Hamiltonian [34], E_i and E_f are the initial and final state energies (including rest masses), and \mathbf{p}_e and \mathbf{p}_ν are the positron/electron and electron-neutrino momenta. The rates for the β^\pm decays and ϵ -capture are given by a similar expression as above, but with the flux factor $1/v$ removed and, in the case of the ϵ -capture, the phase-space integration involves only the outgoing neutrino momenta.

It is convenient to write the averaged weak-interaction Hamiltonian matrix element as $\sum_{ses_\nu} \overline{\sum_{M_1 M_2}} |\langle f | H_W | i \rangle|^2 = (2\pi)^2 G_V^2 L_{\sigma\tau} N^{\sigma\tau}$, where G_V is the Fermi coupling constant ($G_V = 1.14939 \times 10^{-5}$ GeV $^{-2}$), and the lepton tensor $L^{\sigma\tau}$ can be expressed in terms of the positron/electron and neutrino four velocities [35]. The distortion of the charged-lepton wave function in the Coulomb nuclear field is also considered in $L^{\sigma\tau}$ for processes with $A > 4$ [36]. The nuclear tensor $N^{\sigma\tau}$ can be expressed in terms of the reduced matrix elements of the Coulomb, longitudinal, electric and magnetic transition operators, corresponding to the multipole expansion of the nuclear weak current. Since the latter has scalar or vector (V) and pseudoscalar or axial-vector (A) components, each multipole consists of the sum of V and A terms, and the parity of l th multipole V -operators is opposite of that of l th multipole A -operators. The parity of Coulomb, longitudinal, and electric l th multipole V -operators is $(-)^l$, while that of magnetic l th multipole V -operators is $(-)^{l+1}$.

Finally, in later sections, the results for capture reactions between charged clusters will be presented in terms of the astrophysical S -factor, related to the total cross section $\sigma(E)$, via $S(E) = E\sigma(E)\exp(2\pi Z_1 Z_2 \alpha/v)$, where Z_1 and Z_2 are the atomic numbers of the incoming clusters. The exponential factor is the Coulomb penetration factor.

4 The nuclear transition current operators

The model for the nuclear electroweak current has been most recently reviewed in Refs. [33,35]. The current is written as sum of one- and many-body components that operate on the nucleon degrees of freedom. The one-body operators are derived from the nonrelativistic reduction of the covariant single-nucleon electroweak currents and include terms up to order $1/m^2$, where m is the nucleon mass [33,35]. Inclusion of only one-body terms is known as the “impulse approximation” (IA). The two-body operators are discussed briefly in the following two subsections.

4.1 *The electromagnetic two-body currents*

The two-body current has “model-independent” and “model-dependent” components, in the classification scheme of Riska [37]. The model-independent terms are obtained from the two-nucleon interaction and are constructed [38] so as to satisfy current conservation. The leading operator is the isovector “ π -like” current obtained from the isospin-dependent spin-spin and tensor interactions [33]. The same components of the interaction also generate an isovector “ ρ -like” current. Additional model-independent isoscalar and isovector currents arise from the isospin-independent and isospin-dependent momentum-dependent interactions. However, these currents are short-ranged and numerically far less important than the π -like current.

The model-dependent currents are purely transverse and therefore cannot be directly linked to the two-nucleon interaction. Present results include the contributions due to the isoscalar $\rho\pi\gamma$ and isovector $\omega\pi\gamma$ transition currents as well as those due to the isovector current associated with excitation of intermediate Δ resonances. Two different approximations have been used to treat the Δ degrees of freedom [33]; one is based on first-order perturbation theory, using the static Δ approximation, while the other is the transition-correlation-operator (TCO) scheme [39], essentially a scaled-down version of the full $N+\Delta$ coupled-channel method. Comparisons between results obtained within these two approximate schemes have been reported in a number of studies [39,40,41].

The presence of $3N$ interactions in the Hamiltonian requires corresponding three-body currents in order to fulfill current conservation, but these were found to be numerically unimportant in studies of the trinucleon magnetic form factors at intermediate momentum transfer [41].

4.2 *The weak two-body currents*

The nuclear weak current consists of vector (V) and axial-vector (A) parts, with corresponding one- and two-body components. The weak vector current is constructed from the isovector part of the electromagnetic current, in accordance with the conserved-vector-current hypothesis [34].

Some of the two-body axial-current operators are derived from π - and ρ -meson exchanges and the $\rho\pi$ -transition mechanism. These mesonic operators have been found to give rather small contributions in weak transitions involving few-nucleon systems [27,35,42]. The two-body weak axial-charge operator includes a pion-range term from soft-pion theorem and current algebra arguments [43], as well as short-range terms associated with scalar- and vector-meson exchanges. The latter are obtained consistently with the two-nucleon interaction model, following a procedure [44] similar to that used to derive the corresponding weak vector-current operators [35].

The dominant two-body axial current operator, however, is that due to Δ excitation [27,35]. Since the $N\Delta$ transition axial-vector coupling constant g_A^* is not known experimentally, the associated contribution suffers from a large model dependence. To reduce it, g_A^* has been adjusted to reproduce the experimental value of the Gamow-Teller (GT) matrix element in ${}^3\text{H}$ β decay (cf. Table 6). As in the case of the electromagnetic current, the perturbative and TCO approximations have been used to calculate the Δ -excitation axial current contributions. We emphasize that results obtained within the two schemes are typically very close to each other once g_A^* is fixed, for each scheme, to reproduce the ${}^3\text{H}$ GT matrix element (cf. Table XV of Ref. [35]).

Some of our weak transition studies in few-nucleon systems have also been carried out by using weak current operators derived within an effective-field-theory (EFT) approach, in which pions and nucleons are the explicit degrees of freedom and terms up to next-to-next-to-next-to-leading order (N^3LO) are included. Explicit expressions for these EFT operators can be found in Ref. [45]. Here we only note that: i) the two-body operators are regularized by a cutoff that defines the energy/momentum scale of EFT below which the chosen explicit degrees of freedom are valid; ii) the axial-current terms depend on an unknown parameter d_R that gives the strength of a counterterm and is fixed, for a given value of the cutoff, by again reproducing the ${}^3\text{H}$ GT matrix element. The premise of EFT is that physical observables should not depend on the cutoff as long as the latter is chosen in a physically reasonable range. Such an expectation is indeed borne out in the EFT calculation of the pp capture discussed below.

5 Wave functions

Wave functions (bound and continuum) for the present calculations are computed by two means: correlated hyperspherical harmonics (CHH) and variational Monte Carlo (VMC). In the CHH method, the nuclear wave function is expanded on a suitable basis and the unknown expansion parameters are calculated using appropriate variational principles. This technique is very successful in describing nuclear ground states with $A \leq 4$ [46,47,48,49], the Nd scattering states both below and above the deuteron breakup threshold [50,51,52,53,54], and the $p{}^3\text{He}$ and $n{}^3\text{H}$ systems below the ${}^3\text{He}$ and ${}^3\text{H}$

breakup thresholds [55,56]. VMC is an approximate method that uses Monte Carlo sampling to perform numerical quadratures and obtain upper bounds to ground and excited state energies for $3 \leq A \leq 10$ nuclei [6,57]. There is also the Green's function Monte Carlo (GFMC) method that starts from a VMC trial function and employs Monte Carlo integration to evaluate an imaginary-time path integral that projects out exact states of a nucleus. Extension of the Monte Carlo methods to describe continuum states is more difficult, as discussed below, and the GFMC method has not yet been used to compute reaction cross sections.

5.1 Hyperspherical harmonic wave functions for bound states

We first consider the CHH method applied to the $A = 3$ bound state. The wave function Ψ of a three-nucleon system with total angular momentum JM and total isospin TT_z can be written as [46]

$$\Psi = \sum_{\alpha,n} u_{\alpha,n}(\rho) \sum_p H_{\alpha,n}(p) . \quad (8)$$

Here ρ is the hyper-radius, $\rho = (x_i^2 + y_i^2)^{1/2}$, with the Jacobi coordinates \mathbf{x}_i and \mathbf{y}_i defined respectively as $\mathbf{x}_i = \mathbf{r}_j - \mathbf{r}_k$ and $\mathbf{y}_i = (\mathbf{r}_j + \mathbf{r}_k - 2\mathbf{r}_i)/\sqrt{3}$. The index p denotes an even permutation of the particle indices i,j,k . The functions $H_{\alpha,n}$ are antisymmetric under the exchange $j \rightleftharpoons k$. They are given by the product of an angle-spin-isospin function Y_α and a hyperspherical polynomial $P_{\alpha,n}(\phi_i)$, ϕ_i being the hyper-angle defined as $\phi_i = \cos^{-1}(x_i/\rho)$. The index α specifies the set of the spectator i and pair jk orbital angular momenta, l_α and L_α , spin, and isospin, which are coupled to produce the given $JMTT_z$ quantum numbers and the appropriate parity. The $P_{\alpha,n}(\phi_i)$ is proportional to a Jacobi polynomial; the second index n runs over all non-negative integers and specifies the order $K = l_\alpha + L_\alpha + 2n$ of the polynomial. The product of the Jacobi polynomial with the spherical harmonics $Y_{l_\alpha}(\hat{\mathbf{x}}_i)$ and $Y_{L_\alpha}(\hat{\mathbf{y}}_i)$ contained in Y_α is by definition a hyperspherical harmonic function. Finally, correlation factors, which are functions of the jk relative distance, are included in $H_{\alpha,n}$ to account for the strong state-dependent correlations induced by the NN interaction. These correlation functions are solutions of suitable two-body Schrödinger equations [46]. Their presence greatly improves the rate of convergence of the expansion of Eq. (8); the results quoted in this work have been obtained with 23 angle-spin-isospin channels, for which the maximum K is 16 [48]. To obtain a comparable accuracy without correlation factors, the maximum value of K needs to be about 180 [58].

The Rayleigh-Ritz variational principle is used to determine the hyper-radial functions $u_{\alpha,n}(\rho)$ and the ground state energy E . Carrying out the variation $\delta_u \Psi$ with respect to the functions $u_{\alpha,n}(\rho)$, and performing the spin-isospin sums and the integration over the angular and hyper-angular variables yields a set of coupled second-order differential equations for the $u_{\alpha,n}(\rho)$. This is then solved numerically [46,50].

Table 1

Calculated AV18/UIX and experimental binding energies of light nuclei in MeV.

$^A Z(J^\pi; T)$	CHH	VMC(I)	VMC(II)	GFMC	Expt
$^3 \text{H}(\frac{1}{2}^+; \frac{1}{2})$	8.479	8.227(6)		8.461(6)	8.482
$^3 \text{He}(\frac{1}{2}^+; \frac{1}{2})$	7.750	7.476(6)		7.708(6)	7.718
$^4 \text{He}(0^+; 0)$	27.89	27.40(3)		28.31(2)	28.30
$^6 \text{Li}(1^+; 0)$		28.05(5)	28.16(5)	31.25(8)	31.99
$^7 \text{Li}(\frac{3}{2}^-; \frac{1}{2})$		33.07(7)	32.47(7)	37.5(1)	39.24
$^7 \text{Li}(\frac{1}{2}^-; \frac{1}{2})$		33.13(7)	32.23(7)	37.6(1)	38.76
$^7 \text{Be}(\frac{3}{2}^-; \frac{1}{2})$		31.49(7)	30.60(7)	35.9(1)	37.60
$^7 \text{Be}(\frac{1}{2}^-; \frac{1}{2})$		31.58(8)	30.71(7)	35.9(2)	37.17

The extension of the CHH approach to the study of the α -particle is conceptually straightforward but numerically much more involved [47,55]. In analogy with the three-body case, the wave function Ψ is written as in Eq. (8) and the Rayleigh-Ritz variational principle is again used to determine the hyper-radial functions and ground state energy E . However, it should be noted that in the case of $A = 4$, there are two sets of Jacobi coordinates, corresponding to the 1+3 and 2+2 partitions, and both partitions have been used in the definition of the angle-spin-isospin functions Y_α . Furthermore, there are three hyperspherical coordinates, the hyper-radius and two hyper-angles, and only one hyper-angle depends on the partition considered. The hyperspherical polynomial of Eq. (8) depends in this case on two non-negative integers, which specify the order of two individual Jacobi polynomials, functions of the hyper-angles. Finally, the correlation factors are products of pair-correlation functions and are obtained by the same procedure as in the three-body case. More details are given in Ref. [47].

The results for the binding energies of $^3 \text{H}$, $^3 \text{He}$ and $^4 \text{He}$ obtained with the CHH method for the AV18/UIX Hamiltonian are given in Table 1 [35,48]. Note that an accuracy of 1 (10) keV can be achieved for the three-body (four-body) problem.

5.2 Variational Monte Carlo wave functions for bound states

A good VMC wave function, $\Psi_V(J^\pi; A, T)$, is constructed from products of two- and three-body correlation operators acting on an antisymmetric Jastrow wave function with the appropriate quantum numbers:

$$|\Psi_V\rangle = \left[1 + \sum_{i < j < k \leq A} U_{ijk}^{TNI} \right] \left[\mathcal{S} \prod_{i < j \leq A} (1 + U_{ij}) \right] |\Psi_J\rangle. \quad (9)$$

Here \mathcal{S} denotes symmetrization over the noncommuting pair correlation operators U_{ij} , which include spin, isospin, and tensor terms, $U_{ij} = \sum_{p=2,6} u_p(r_{ij}) O_{ij}^p$, and O_{ij}^p are the same static operators that appear in the NN potential, Eq.(2). The U_{ijk}^{TNI} are correlations induced by the three-nucleon interaction, and have the same spin-isospin structure as the V_{ijk} of Eq.(4).

The Jastrow wave function, Ψ_J , for s-shell nuclei has the simple form

$$|\Psi_J\rangle = \left[\prod_{i < j < k \leq A} f_{ijk}^c \right] \left[\prod_{i < j \leq A} f_c(r_{ij}) \right] |\Phi_A(JMTT_z)\rangle . \quad (10)$$

Here $f_c(r_{ij})$ and f_{ijk}^c are central two- and three-body correlation functions and Φ_A is a Slater determinant in spin-isospin space, e.g., for the α -particle, $|\Phi_4(0000)\rangle = \mathcal{A}|p \uparrow p \downarrow n \uparrow n \downarrow\rangle$. The functions $f_c(r)$ and $u_p(r)$ are generated by solving a set of coupled differential equations containing the bare NN potential with appropriate asymptotic boundary conditions [59]. Variational parameters in these equations are adjusted to minimize the energy expectation value, $E_V = \langle \Psi_V | H | \Psi_V \rangle$, which is evaluated by Metropolis Monte Carlo integration [60].

The Ψ_J for p-shell nuclei is more complicated, with single-nucleon p-shell orbitals and LS coupling to obtain the desired JM value [61]. We sum over all allowed spatial symmetries $[n]$ [62] and allow for three types of central pair correlations depending on which shell the nucleons are in:

$$|\Psi_J\rangle = \mathcal{A} \left\{ \prod_{i < j < k \leq 4} f_{ijk}^c \prod_{i < j \leq 4} f_{ss}(r_{ij}) \sum_{LS[n]} \left(\beta_{LS[n]} \prod_{k \leq 4 < l \leq A} f_{sp}^{LS[n]}(r_{kl}) \right. \right. \\ \left. \left. \prod_{4 < l < m \leq A} f_{pp}^{LS[n]}(r_{lm}) \right) |\Phi_A(LS[n]JMTT_z)_{1234:5...A}\rangle \right\} . \quad (11)$$

The operator \mathcal{A} indicates an antisymmetric sum over all possible partitions into 4 s-shell and $(A - 4)$ p-shell particles. The pair correlation for both particles within the s-shell, f_{ss} , is similar to the f_c of the α -particle. The pair correlations for both particles in the p-shell, $f_{pp}^{LS[n]}$, and for mixed pairs, $f_{sp}^{LS[n]}$, are similar to f_{ss} at short distance, but their long-range structure is adjusted to give appropriate clustering behavior, and they may vary with $LS[n]$. The single-particle wave function components are:

$$|\Phi_A(LS[n]JMTT_z)_{1234:5...A}\rangle = |\Phi_4(0000)_{1234}\rangle \times \left| \prod_{4 < l \leq A} \phi_p^{LS[n]}(R_{\alpha l}) \right. \quad (12) \\ \left. \left\{ \left[\prod_{4 < l \leq A} Y_{1m_l}(\Omega_{\alpha l}) \right]_{LM_L[n]} \times \left[\prod_{4 < l \leq A} \chi_l(\frac{1}{2}m_s) \right]_{SM_S} \right\}_{JM} \times \left[\prod_{4 < l \leq A} \nu_l(\frac{1}{2}m_t) \right]_{TT_z} \right\rangle .$$

The $\phi_p^{LS[n]}(R_{\alpha l})$ are p-wave solutions of a particle in an effective α - N potential that has Woods-Saxon and Coulomb parts. They are functions of the distance between the center of mass of the α -core and nucleon l , and may vary with $LS[n]$. The wave function is translationally invariant, so there is no spurious

center of mass motion.

Two different types of Ψ_J have been constructed in recent VMC calculations of light p-shell nuclei: Type I, which is a shell-model trial function [63], and Type II, which is a cluster-cluster trial function [64,65]. In Type I trial functions, the $\phi_p^{LS[n]}(r)$ has an exponential decay at long range, with the depth, range, and surface thickness of the Woods-Saxon potential serving as variational parameters. The $f_{sp}^{LS[n]}$ go to a constant near unity at long range, while the $f_{pp}^{LS[n]}$ have a small long-range tail that is larger for states of lesser spatial symmetry $[n]$ [63]. In Type II trial functions, $\phi_p^{LS[n]}(r)$ is again the solution of a p-wave Schrödinger equation with a potential containing Woods-Saxon and Coulomb terms, but with an added Lagrange multiplier that turns on at long range and imposes the boundary condition $[\phi_p^{LS[n]}(r \rightarrow \infty)]^n \propto W_{km}(2\gamma r)/r$. Here $W_{km}(2\gamma r)$ is the Whittaker function for bound-state wave functions in a Coulomb potential and n is the number of p-shell nucleons. The cluster separation wave number γ is taken from experiment. The accompanying $f_{sp}^{LS[n]}$ goes to unity while the $f_{pp}^{LS[n]}$ are taken from the exact deuteron wave function in the case of ${}^6\text{Li}$, or the VMC ${}^3\text{H}$ (${}^3\text{He}$) Ψ_V in the case of ${}^7\text{Li}$ (${}^7\text{Be}$). Consequently, Type II trial functions factorize at large cluster separations as $\Psi_V \rightarrow \psi_\alpha \psi_\tau W_{km}(2\gamma r_{\alpha\tau})/r_{\alpha\tau}$, where ψ_α and ψ_τ are the wave functions of the clusters and $r_{\alpha\tau}$ is the separation between them [64,65].

For either type of trial function, a diagonalization is carried out in the one-body basis to find the optimal values of the $\beta_{LS[n]}$ mixing parameters for a given $(J^\pi; T)$ state. Current best VMC energies for nuclear states of astrophysical interest are given in Table 1 for the AV18/UIX Hamiltonian along with CHH and GFMC results and experimental values. These VMC results are about 1 MeV more bound for $A=6,7$ nuclei than previously reported because of recent improvements in the parametrization of the trial functions; however, results for various transition matrix elements are not significantly altered. The VMC energies for $A=3,4$ nuclei are 1–2% above CHH or GFMC results, but are 10–15% higher for $A=6,7$ than GFMC results, which are themselves 5% high compared to experiment with this Hamiltonian.

5.3 Hyperspherical harmonic wave functions for continuum states

The CHH method has also been applied to the study of scattering problems. In particular, pd and nd systems have been studied both below [50,51] and above [52,53,54] the deuteron breakup threshold. The $p\,{}^3\text{He}$ and $n\,{}^3\text{H}$ systems have also been investigated below the ${}^3\text{He}$ (${}^3\text{H}$) breakup threshold [55,56]. We now review how the CHH method works for the $N + A$ scattering below the mass- A nuclear breakup threshold.

The wave function Ψ_{N+A}^{LSJM} , having incoming orbital angular momentum L and spin S coupled to total JM , is written as the sum of a core function Ψ_c^{JM} and an asymptotic function Ψ_a^{LSJM} . The function Ψ_c describes the system in the region where the particles are close to each other and their mutual

Table 2

Calculated $A = 3$ doublet (a_d) and quartet (a_q), and $A = 4$ singlet (a_s) and triplet (a_t) scattering lengths in fm [40,55]. Experimental results are from Refs. [67,68].

	nd		pd		$n\ ^3\text{H}$		$p\ ^3\text{He}$	
	a_d	a_q	a_d	a_q	a_s	a_t	a_s	a_t
CHH	0.63	6.33	-0.02	13.7	4.32	3.80	11.5	9.13
Expt	0.65(4)	6.35(2)				10.8(2.6)	8.1(5)	

interactions are large, and vanishes in the limit of large inter-cluster separation. It is obtained by an expansion on the same CHH basis as discussed above for the bound state. In the asymptotic region the inter-cluster interactions are negligible, and Ψ_a^{LSJM} is written as (in the $p + A$ case)

$$\begin{aligned} \Psi_a^{LSJM} = & \sum_i \sum_{L'S'} \left[[s_i \otimes \phi_A]_{S'} \otimes Y_{L'}(\hat{\mathbf{r}}_{pA}) \right]_{JM} \\ & \times \left[\delta_{LL'} \delta_{SS'} \frac{F_{L'}(kr_{pA})}{kr_{pA}} + R_{LS,L'S'}^J(k) \frac{G_{L'}(kr_{pA})}{kr_{pA}} g(r_{pA}) \right] . \end{aligned} \quad (13)$$

Here ϕ_A , \mathbf{r}_{pA} and k are the mass- A cluster wave function, the proton and A -cluster relative distance, and the magnitude of the relative momentum, respectively. The functions F_L and G_L are the regular and irregular Coulomb functions, respectively. For $n+A$ scattering, $F_L(x)/x$ and $G_L(x)/x$ are replaced by the regular and irregular spherical Bessel functions. The function $g(r_{pA})$ regularizes $G_L(kr_{pA})$ at $r_{pA} = 0$, and $g(r_{pA}) \rightarrow 1$ as $r_{pA} \geq 10 - 12$ fm. Finally $R_{LS,L'S'}^J(k)$ are the R -matrix elements that determine phase shifts and (for coupled channels) mixing angles at the energy $k^2/(2\mu)$, μ being the $N + A$ reduced mass. The sum over $L'S'$ includes all values compatible with a given total J and parity. Both the matrix elements $R_{LS,L'S'}^J(k)$ and the hyper-radial functions occurring in the expansion of Ψ_c are determined by applying the Kohn variational principle.

The nd , pd , and $p\ ^3\text{He}$ scattering lengths predicted by the AV18/UIX model are shown in Table 2 [40,55]. Also listed in the table are the $n\ ^3\text{H}$ scattering lengths predicted by the older AV14/UVIII Hamiltonian [59,66]. There is excellent agreement between the theoretical predictions and the available data.

5.4 Phenomenological continuum states for $A > 4$

Few calculations of continuum states consisting of two nuclei have been done in the quantum Monte Carlo formalism, and several difficulties in these calculations remain to be addressed. We expect these problems to be tractable, and work on them continues. In the meantime, we have adopted a semi-phenomenological prescription for the continuum-state wave functions that enter into capture calculations for the $A > 4$ systems [64,65].

At large separations between nuclei in a continuum state, the wave function

is the product of the wave functions ϕ_1 and ϕ_2 of the two nuclei with a two-body correlation that describes the (nuclear plus Coulomb) scattering of the two nuclei from each other. This is

$$\Psi_{A_1+A_2}^{LSJM} \propto \left[[\phi_1 \otimes \phi_2]_S \otimes Y_L(\hat{\mathbf{r}}_{12}) \right]_{JM} \left[\frac{F_L(kr_{12})}{kr_{12}} + \tan \delta_{LSJ}(k) \frac{G_L(kr_{12})}{kr_{12}} \right], \quad (14)$$

where r_{12} is the separation between the initial nuclei. This is analogous to Eq.(13) without coupled channels, and the angular momentum labels have the same meanings.

To obtain approximate continuum wave functions, we have adopted the form

$$\Psi_{A_1+A_2}^{LSJM} = \mathcal{A} \psi_{12}^{LSJ}(r_{12}) \prod_{ij} G_{ij} \left[[\phi_1 \otimes \phi_2]_S \otimes Y_L(\hat{\mathbf{r}}_{12}) \right]_{JM} \quad (15)$$

for the wave function. The operator \mathcal{A} antisymmetrizes the wave function under exchange of nucleons between the two (internally antisymmetric) clusters. The short-range G_{ij} operator correlations between nucleon pairs in different clusters produces distortions in the nuclei when they occupy the same space, and they go to unity at less than 2 fm interparticle separation. We used correlations G_{ij} found in nuclear-matter calculations [69] and found that they had essentially no effect on the cross sections.

We generated the radial function $\psi_{12}^{LSJ}(r_{12})$ from a Schrödinger equation

$$\left\{ \frac{\hbar^2}{2\mu_{12}} \left[-\frac{d^2}{dr_{12}^2} + \frac{L(L+1)}{r_{12}^2} \right] + V_{LSJ}(r_{12}) \right\} (r_{12} \psi_{12}^{LSJ}) = E(r_{12} \psi_{12}^{LSJ}). \quad (16)$$

The appropriate reduced mass for the nuclei is μ_{12} . The effective potential function $V_{LSJ}(r_{12})$ was chosen to be the sum of a short-range nuclear interaction (Woods-Saxon or similar, with central and spin-orbit terms) and the Coulomb interaction. We chose $V_{LSJ}(r_{12})$ to reproduce the experimentally determined phase shifts $\delta_{LSJ}(k)$. For both $A = 6$ and $A = 7$ α -captures, several suitable choices of V_{LSJ} were already available in the literature, so we chose from among those [7,8,9,10,70,71,72], making minor adjustments to reproduce the well-known width and location of the 3^+ resonance in ${}^6\text{Li}$. The dependence of our results on the different V_{LSJ} indicates the amount of uncertainty introduced by this approach. To satisfy the Pauli principle, the functions V_{LSJ} need deep potential wells with forbidden states to produce the correct number of nodes in ψ_{12}^{LSJ} [73], as well as parity dependence. The ${}^6\text{Li}$ V_{LSJ} also contains a spin-orbit term to describe three low-lying resonances important for the radiative capture. It can in principle also admit a tensor interaction (requiring modification of Eqs.(14) and (16)), but it is not unambiguously required by the data, and we did not include it.

The $J^\pi = 1^+$ wave functions in αd should also be to be orthogonal to the ${}^6\text{Li}$ ground state, but there is no guarantee of this in the present approach because ψ_{12}^{LSJ} was not obtained from the underlying NN interaction. We found

that this property is only important for magnetic dipole transitions proceeding from S waves. For this matrix element, we kept only the part of $\Psi_{A_1+A_2}^{LSJM}$ orthogonal to the VMC ground state.

Finally, the states ϕ_1 and ϕ_2 appearing in Eq.(15) were computed directly from the two- and three-nucleon forces by the VMC method, except that the deuteron wave function ϕ_d was a direct numerical solution of the two-body Schrödinger equation for the deuteron.

6 Results

6.1 The $p(n,\gamma)d$ radiative capture below 1 MeV

Historically, the radiative capture of thermal neutrons on protons played a crucial role in establishing the quantitative importance of two-body current effects in photonuclear observables [74]. Their inclusion resolved the long-standing discrepancy between the calculated impulse approximation (IA) cross section and the measured value. In this section, we briefly summarize the results of cross section calculations for this process from thermal energies up to energies of $\simeq 1$ MeV; the energy range between a few tens of keV up to 200 keV is particularly relevant for primordial nucleosynthesis.

At thermal energy, the cross section σ^γ is due to the well-known isovector magnetic dipole (M_1) transition connecting the 1S_0 np scattering state to the deuteron bound state. There is in principle an isoscalar M_1 transition proceeding through the 3S_1 np continuum state, but the associated contribution (at thermal energy) is strongly suppressed in IA by orthogonality; furthermore, isoscalar two-body currents, such as those originating from the momentum-dependent components of the two-nucleon interaction or from the $\rho\pi\gamma$ transition mechanism, are numerically far less important than isovector currents, and play a very marginal role in this transition.

The calculated values for σ^γ are listed in Table 3, both for one-body currents alone and for the one- and two-body currents. The IA results are to a large extent determined by the 1S_0 scattering length and deuteron binding energy, which the above interactions reproduce exactly. Indeed, in effective range theory, one finds that $\sigma^\gamma \simeq 300$ mb. Among the two-body current contributions, which collectively amount to approximately 9% of the total cross section, the largest one, about 60%, comes from the currents associated with pion exchange. The next to largest, about 25%, is from currents involving Δ excitation, that have been treated in perturbation theory here.

As the energy increases from a few to several hundreds of keV, contributions to σ^γ from the electric dipole (E_1) transitions proceeding through the 3P_J np scattering states become more important, and in fact dominant at energies larger than 300 keV. The Siegert form is used for the E_1 operator, and relativistic corrections to the charge density, such as those associated with spin-orbit and pion-exchange contributions [76,64], have been neglected.

Table 3

Total cross-section σ^γ in mb for thermal np radiative capture; data from Ref. [75].

NN model	AV18	Nijm-I	CD-Bonn	Expt
One-body	304.6	305.4	306.5	
Full	334.2	332.5	331.6	332.6(7)

The results of calculations based on the AV18 and CD-Bonn interactions are shown in Fig. 1. As the energy increases the model dependence, already less than 1% at thermal energies, becomes negligible at 1 MeV, where the E_1 contribution dominates. This is to be expected, since the E_1 transition is mostly sensitive to the long-range part of the wave functions. Fig. 1 demonstrates that the model dependence of the predictions in the conventional approach based on realistic interactions is considerably less than 1% in the energy range relevant for primordial nucleosynthesis. It could be further reduced by adjusting, for example, the transition magnetic moment $\mu_{\gamma N \Delta}$ of the Δ -excitation current to precisely fit the thermal neutron capture cross section. In all results reported so far $\mu_{\gamma N \Delta}$ has been taken to be 3 nm, a value consistent with an analysis of γN data at resonance.

Finally, it is worth emphasizing that the model dependence referred to above is comparable to the theoretical uncertainty inherent in calculations based on effective field theory [77,78]. These calculations involve contact operators whose strength has to be constrained by experimental data. In the more recent study of Ref. [78], for example, there is a contact four-nucleon-photon operator, whose M_1 (E_1) strength is fixed by the measured thermal capture cross section (deuteron photo-disintegration data at threshold).

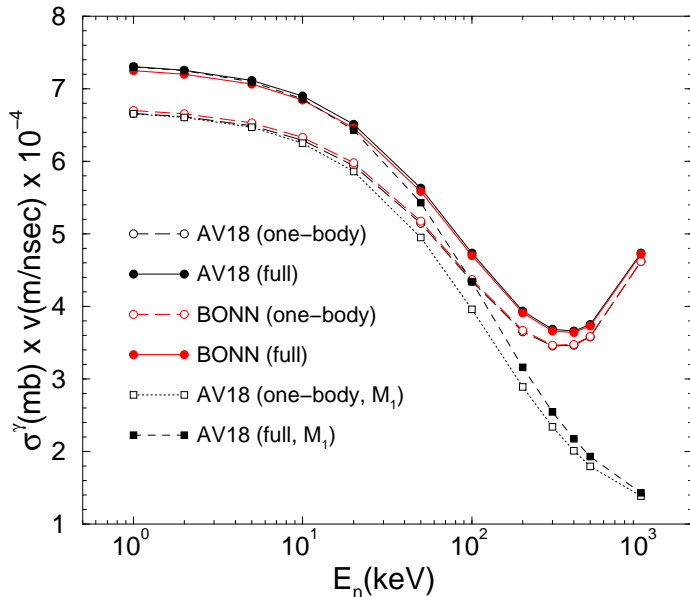


Fig. 1. Predictions for np radiative capture cross section, calculated with the AV18 and CD-Bonn interactions. Also shown for AV18 is the M_1 contribution to σ^γ .

Table 4

Square of the overlap integral $\Lambda(E = 0)$ for five modern NN interaction models.

NN model	AV18	Nijm-I	Nijm-II	Reid93	CD-Bonn
Λ^2 (one-body)	6.965	6.965	6.971	6.974	6.985
Λ^2 (full)	7.076				7.060

6.2 The pp weak capture

The theoretical description of the proton weak capture on protons was first given by Bethe and Critchfield [22], who showed that the associated rate was large enough to account for the energy released by the sun. Since then, a series of calculations have refined their original estimate either by computing the required wave functions more accurately [79,80,81,82] or by using more realistic models for the nuclear transition operator [83,84,85]. However, the most recent studies [27,45] offer an integrated treatment of these two aspects with emphasis on a reliable estimate of their associated uncertainties.

The pp weak capture is induced by the weak axial current operator, and the S -factor is conventionally written in terms of a dimensionless parameter $\Lambda(E)$ [27], where E is the pp relative energy. When axial two-body currents are neglected, it is given by

$$\Lambda(E) = \left(\gamma^3/2\right)^{1/2} \frac{1}{C_0(k) k} \int_0^\infty dr u(r) \chi_0(r; k) , \quad (17)$$

where γ is the deuteron wave number, k is the pp relative momentum ($E=k^2/m_p$), and $C_0(k)$ is the Gamow penetration factor. In the overlap integral, $u(r)$ is the S-wave component of the deuteron wave function and $\chi_0(r; k)$ is the pp 1S_0 continuum wave function. The 1S_0 wave function is the solution of a Schrödinger equation with a pp interaction including, in addition to the nuclear and Coulomb terms, terms of second order in the fine structure constant. These are the vacuum polarization and two-photon exchange terms, as well as corrections originating from the finite size of the proton [27]. Properly accounting for these additional electromagnetic interaction components leads to some practical problems in integrating the Schrödinger equation, matching the Coulomb functions, and extracting the phase shift. The most important correction to the Coulomb interaction between protons is the vacuum polarization, which reduces the cross section (proportional to Λ^2) by about 1%. Other fine details of the electromagnetic interaction increase the cross section by about 0.1%. This is in part canceled by a net 0.03% reduction in cross section from the correct relativistic treatment of the deuteron wave number, γ . Including just the axial one-body operator, five modern interaction models differ by only 0.3% in the calculated cross section as illustrated in Table 4.

The model for the axial two-body current contains the simplest possible two-body operators that give an adequate description of the longest-range

mechanisms. The overall strength of the leading operator due to Δ excitation is adjusted as described in Sec. 4.2. The contributions due to exchanges of heavier mesons, such as the A_1 [86], or renormalization effects arising from Δ admixtures in the nuclear wave functions [39], are neglected. However, in Ref. [27] it was shown that these approximations do not influence in any significant way the theoretical predictions for the pp weak capture cross section once the two-body current model is constrained to fit the GT matrix element of tritium.

The results for $\Lambda^2(0)$ including axial two-body currents are listed for the AV18 and CD-Bonn interactions in Table 4. Predictions for this quantity with other modern interactions are expected to be similar. Thus, the model dependence and theoretical uncertainty appear to be at the level of a few parts in a thousand, much smaller than the estimate given in Ref. [23].

More recently [45], the pp (and *hep*, see below) astrophysical rates have been calculated using wave functions obtained from solutions of the Schrödinger equation with realistic interactions, and axial two-body currents derived from chiral effective field theory (EFT), as discussed at the end of Sec. 4.2. In Ref. [45], the pp *S*-factor is the physical observable chosen to test the energy/momentum cutoff dependence. It has been demonstrated that this observable is independent of the cutoff as long as its value is within a physically reasonable range. In particular, this work gives for the ratio of the two-body to one-body contributions the value $(0.86 \pm 0.05)\%$, in line with the results of the conventional theory reported above.

6.3 The $d(n, \gamma)^3H$ and $d(p, \gamma)^3He$ radiative captures

The theoretical description of the $A=3$ and 4 radiative and weak capture processes constitutes a challenging problem for nuclear few-body theory [35,33,39,87,88]. The difficulty comes about because the $A=3$ and 4 bound states are approximate eigenstates of the M_1 and GT one-body operators [89]. This property would be exact if these states were to consist only of a symmetric S-wave component, which accounts for over 90% (80%) of the $A=3$ (4) bound states. It is spoiled by the presence of D-state components induced by tensor interactions. Consequently, the one-body matrix elements of these (largely) M_1 - or GT-induced processes are suppressed due to orthogonality between the initial and final states. As a result, the associated cross sections become extremely sensitive to contributions from small components in the wave functions and two-body electroweak current operators.

The extensive experimental data for the $d(n, \gamma)^3H$ and $d(p, \gamma)^3He$ reactions include both total cross sections and spin polarization observables at several center-of-mass energies. The most complete comparison between theory and experiment for the $d(n, \gamma)^3H$ and $d(p, \gamma)^3He$ radiative captures below the deuteron breakup threshold was performed using CHH wave functions obtained from the AV18/UIX interaction [40,76], with a nuclear electromagnetic current operator that includes both one- and two-body contributions. The

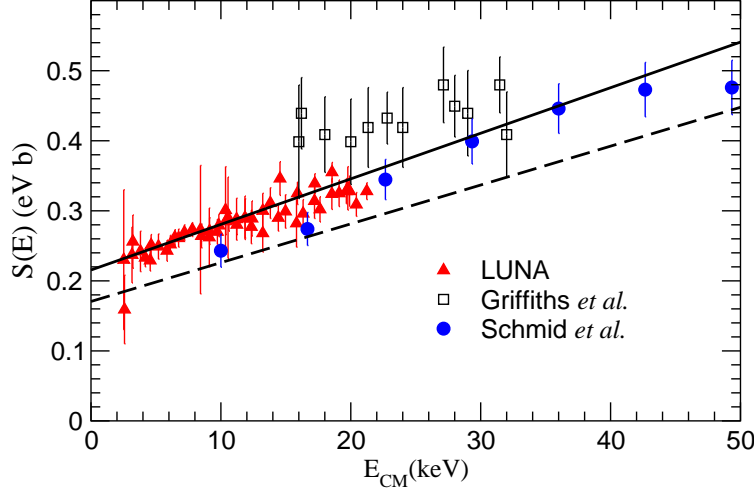


Fig. 2. The calculated S -factor [76] for $d(p, \gamma)^3\text{He}$ obtained using AV18/UIX CHH wave functions and one-body only (dashed line) or both one- and two-body (solid line) currents. Experimental data are taken from Refs. [94,95,96,97].

proton radiative capture calculation has been extended above the deuteron breakup threshold [90,91,92], but we consider only the low-energy regime.

The theoretical prediction of Ref. [40] for the total cross section σ_T of thermal $d(n, \gamma)^3\text{H}$ is 0.578 for the full and 0.229 mb for the impulse approximation (IA) current operators. The experimental value is $\sigma_T = 0.508 \pm 0.015$ mb [93]. Therefore, the “full” result, while clearly an improvement over the IA, still exceeds the experimental value by 14%. The origin of this discrepancy is puzzling, particularly in view of the fact that the astrophysical S -factor for the related dp radiative capture at zero energy is calculated to be within 1% of the measured value (see below).

The calculated S -factor [76] in the energy range 0–50 keV is compared with the experimental data of Refs. [94,95,96,97] in Fig. 2. The solid curve represents the “full” result, while the dashed line is the result in IA. The agreement between theoretical predictions and experimental data, especially the very recent LUNA data [94], is excellent. The two-body contributions to the nuclear electromagnetic current operator play a very important role in this agreement. The “full” (IA) theoretical value for $S(0)$ has been found to be 0.219 (0.162) eV·b, in excellent agreement with the LUNA result of 0.216 ± 0.010 eV·b. The theoretical and experimental S -factors also agree nicely at higher energies, as shown in Refs. [90,92] in the energy range 0–2 and 0–3.33 MeV.

6.4 The hen and hep reactions

The total cross section of the $^3\text{He}(n, \gamma)^4\text{He}$ (*hen*) reaction is experimentally known [98], while the astrophysical S -factor of the $^3\text{He}(p, e^+ \nu_e)^4\text{He}$ (*hep*) reaction cannot be directly measured in the energy range relevant for solar fusion. The most recent *ab initio* calculation of the *hen* reaction was performed more

than a decade ago in Refs. [39,87], using VMC wave functions obtained with the older AV14/UVIII Hamiltonian model. The total cross section at thermal neutron energy was found to be $85.9 \mu\text{b}$ when one- and two-body contributions to the electromagnetic current are included, and $5.65 \mu\text{b}$ in IA. The most recent experimental determination gives $55 \pm 3 \mu\text{b}$ [98]. The discrepancy between theory and experiment could indicate that: i) the VMC wave functions obtained with the AV14/UVIII interaction model are not sufficiently accurate; and/or ii) the model for the electromagnetic current needs to be refined. Work currently under way to construct more accurate CHH wave functions for the four-nucleon states involved in the *hen* reaction will help to clarify this issue.

The Super-Kamiokande (SK) measurements of the energy spectrum of electrons recoiling from scattering with solar neutrinos [99,100,101,102] have brought new interest in the *hep* reaction. The first SK results for this spectrum showed an apparent excess of events in the highest-energy bin [100] that could be explained by increasing by a factor of $\simeq 17$ the Standard Solar Model (SSM98) prediction [103] of the *hep* neutrino flux. The most recent results from SK are essentially the same after taking the large mixing angle (LMA) neutrino mixing parameters into account. However, when the quasi-vacuum solution is used, the inferred flux at the earth is reduced by a factor of 4. The *hep* neutrino flux is directly proportional to the *S*-factor at zero energy $S(0)$, and the SSM98 estimate for the flux was based on the calculation of Ref. [39]. This calculation used AV14/UVIII VMC wave functions, retained only the $p^3\text{He } ^3S_1$ channel, neglected the dependence on the momentum transfer of the lepton pair, and used poorly-constrained two-body contributions to the nuclear axial current operator.

Because of the significant progress made with the CHH method in the description of the four-nucleon bound and continuum states [47,55], the *hep* reaction has been re-examined in Refs. [35,88] and Ref. [45]. All S- and P-wave capture states are calculated, using AV18/UIX interaction and retaining the q -dependence of the nuclear weak transition operator. In Refs. [35,88] the TCO model for the weak current is used, while in Ref. [45] the EFT model is used, as discussed in Sec. 4.2. The momentum cutoff Λ was varied between 500 and 800 MeV. The results for $S(0)$ summarized in Table 5 show that the P-wave capture channels are very important and give about 33% of the calculated *S*-factor. Contributions from the D-wave channels are expected to be small [35,88]. The Λ dependence in the 3S_1 channel is the result of the large cancellation between the one-body and the two-body contributions found in Refs. [35,39,88]; such dependence is much smaller in all other channels.

The energy dependence of the *hep* *S*-factor was found in Refs. [35,88] to be rather weak at 0, 5 and 10 keV. In fact, the calculated *S*-factor at 10 keV, close to the *hep* solar Gamow peak, is $10.1 \times 10^{-20} \text{ keV}\cdot\text{b}$, only 4% larger than that at 0 keV. In Ref. [35], $S(0)$ was also calculated using the AV18 and the AV14/UVIII interaction models. The AV14/UVIII (AV18) result is 4% (20%) larger than that for AV18/UIX, demonstrating the need to use a Hamiltonian that accurately reproduces the properties of the three- and four-nucleon bound

Table 5

Contributions to $S(0)$ for hep from individual partial waves in units of 10^{-20} keV·b.

Λ (MeV)	1S_0	3S_1	3P_0	1P_1	3P_1	3P_2	Total	
500	0.02	7.00	0.67	0.85	0.34	1.06	9.95	
Ref. [45]	600	0.02	6.37	0.66	0.88	0.34	1.06	9.37
	800	0.02	4.30	0.66	0.91	0.34	1.06	7.32
Ref. [35,88]		0.02	6.38	0.82	1.00	0.30	0.97	9.64

and scattering states.

Following the results of Refs. [35,88], the Standard Solar Model prediction for the hep neutrino flux has been recently readjusted to be 9.3×10^3 cm $^{-2}$ s $^{-1}$ [104], 4.4 times larger than the SSM98 prediction, but still about 4 times smaller than the latest SK result based on LMA [102].

6.5 The $d(\alpha, \gamma)^6\text{Li}$ radiative capture

The reaction $d(\alpha, \gamma)^6\text{Li}$ is isoscalar, so direct E_1 transitions are suppressed. The M_1 transition from S-wave initial states is also suppressed because the ground state is an approximate eigenstate of the M_1 operator. As a result, the reaction at most energies between 0.2 and 3 MeV is almost purely E_2 in nature, arising from the D waves. The cross section is in the nanobarn range and difficult to measure. Nonetheless, there are two sets of cross section measurements [105,106], and one set of capture cross sections inferred from the breakup process $^{208}\text{Pb} + ^6\text{Li} \rightarrow ^{208}\text{Pb} + \alpha + d$ [46]. This small cross section helps preclude significant production of ^6Li in the big bang.

We show our computed cross sections [64] with the data in Fig. 3. These calculations include all initial states with $L \leq 3$ and the M_1, M_2, E_1, E_2 , and E_3 operators. The two sets of theory curves correspond to two different choices of V_{LSJ} to generate the inter-cluster correlation $\psi_{ad}^{LSJ}(r_{ad})$ of Eq.(16). There is very little dependence on V_{LSJ} , probably because it is well-constrained in the D waves by low-lying resonances.

The total cross sections provide a good match to the data at the narrow 3^+ resonance at 711 keV, partly because V_{LSJ} was adjusted to produce the location and width of this resonance accurately [107] in the scattering phase shifts. At energies between the resonance and 3 MeV, the energy dependence of the cross section provides a good fit to the Robertson data [105]. Beyond 3 MeV, the model fails to reproduce the data, probably because of omitted couplings to channels of nonzero isospin. To match the normalization of the data, our curve would have to be renormalized by a factor 0.85, and the residuals of the data with respect to the renormalized curve are of the order of 10% even for the higher-quality of the two data sets reported in Ref. [105]. We conclude that the theoretical model has come out quite well. This probably reflects a good asymptotic normalization coefficient for projection of the ^6Li

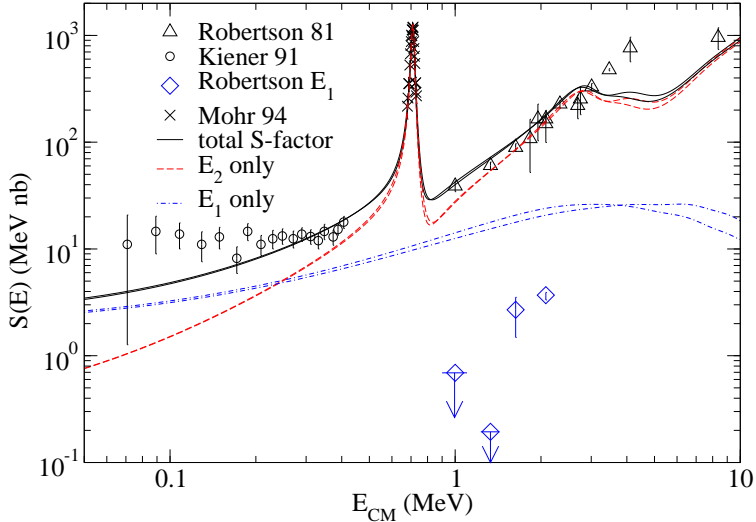


Fig. 3. S -factor for the process $d(\alpha, \gamma)^6\text{Li}$, showing the variation in theoretical curves due to choice of V_{LSJ} . See text for a discussion of the Robertson E_1 [105] points.

ground state onto αd cluster states.

In the region below 500 keV, there are only indirect cross sections (and a rather high upper limit[108]) for comparison, inferred from the process $^{208}\text{Pb} + ^6\text{Li} \rightarrow ^{208}\text{Pb} + \alpha + d$ [109]. This energy range is very interesting, because at about 250 keV, we compute the isoscalar E_1 transition to be half of the total cross section. It becomes more important at lower energies, as the centrifugal barrier disfavors the E_2 contributions arising from the D waves. We do not find the same energy dependence as the indirect measurements, despite our inclusion of terms up to third order in the long-wavelength approximation (LWA) E_1 operator that are important because of the isoscalar transition. The energy dependence of the data suggests S-wave capture, but we compute the cross section for E_2 capture from the S wave to be two orders of magnitude smaller. The angular distributions of the breakup data are consistent with purely E_2 transitions, but the technique also gives much less weight to E_1 transitions than to E_2 .

Although the E_1 operator makes a small contribution to the total cross section above 1 MeV, it interferes with the dominant E_2 amplitudes to produce a forward-backward asymmetry in the distribution of emitted photons. It is a persistent difficulty of capture models that they agree with the laboratory data on neither the sign nor the magnitude of the asymmetry[105,110]. Ours also disagrees with the data, despite the inclusion of several corrections to the LWA E_1 operator, because the leading effect remains the center-of-energy effect arising from the difference in mass per nucleon between the two initial-state nuclei. We note, though, that the upper limits on asymmetry at 1.0 and 1.63 MeV are much smaller than one would expect from extrapolating to lower energies the E_1 contribution measured at 2 MeV in essentially any capture model. This suggests that the shortcoming may be in the data.

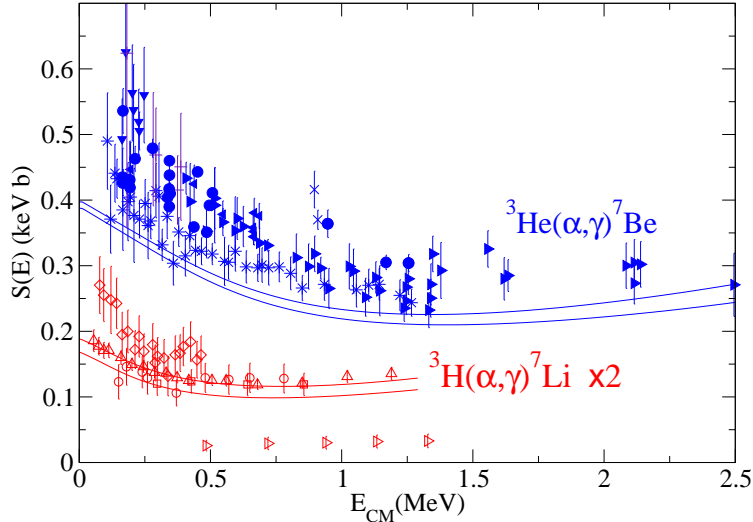


Fig. 4. S -factors for α captures forming ${}^7\text{Li}$ and ${}^7\text{Be}$, showing the spread in the computed values due to choice of V_{LSJ} ; values for ${}^3\text{H}(\alpha, \gamma){}^7\text{Li}$ are multiplied by 2.

6.6 The ${}^3\text{He}(\alpha, \gamma){}^7\text{Be}$ and ${}^3\text{H}(\alpha, \gamma){}^7\text{Li}$ radiative captures

The α -capture processes ${}^3\text{He}(\alpha, \gamma){}^7\text{Be}$ and ${}^3\text{H}(\alpha, \gamma){}^7\text{Li}$ are closely related, and have also been computed by the VMC method [65]. We used the same phenomenological potentials V_{LSJ} of Sec. 5.4 to describe the continuum in both systems, except that the charges in the Coulomb terms and the reduced masses were adjusted to match each system. Both processes are E_1 transitions, originating from S waves at the lowest energies and also partly from D waves at the higher end of the energy range shown in Fig. 4. We computed operators for the same L range and multipolarities as for $d(\alpha, \gamma){}^6\text{Li}$ and found that no transitions besides E_1 matter above the 0.1% level for either reaction. Corrections to the LWA E_1 operator are also negligible (though the center-of-energy correction, omitted because it is expensive to compute, should be on the order of 3% in these cross sections). For both reactions, capture may occur into either of two bound states, with a branching ratio of roughly 0.4.

The computed cross sections [65] for the process ${}^3\text{H}(\alpha, \gamma){}^7\text{Li}$ are shown and compared with the data [111,112,113,114] in Fig. 4. By far the most precise experiment to measure this cross section is that of Brune et al. [115] (upward-pointing open triangles in Fig. 4). Our results for this reaction have a dispersion of about $\pm 5\%$ among calculations for different choices of cluster-cluster potential V_{LSJ} . This dispersion, wider than for $d(\alpha, \gamma){}^6\text{Li}$ or ${}^3\text{He}(\alpha, \gamma){}^7\text{Be}$, probably reflects a substantial contribution to the capture from small $\alpha{}^3\text{H}$ separations. Taking account of this dispersion and of a roughly 10% normalization uncertainty from our Monte Carlo integration, we are in excellent agreement with all the modern data. The ratio of the cross section for capture into the excited state of ${}^7\text{Li}^*$ to that for the ground state is almost independent of V_{LSJ} . While the calculation reproduces the approximate absence of energy dependence seen in the branching ratio data, the predicted ratio itself is about 15%

below the data. (The branching data have a 4% normalization uncertainty.)

The computed energy dependence of the ${}^3\text{H}(\alpha, \gamma){}^7\text{Li}$ total cross section agrees reasonably well with the Brune data, for a reduced χ^2 of 2.5. This compares favorably with other calculations in the literature. At the highest-energy data points, where the S -factor is increasing due to a growing contribution from D-wave capture, our calculation has a slightly shallower energy dependence than the data. We also find a significantly shallower slope for the S -factor at zero energy than all but one other theoretical calculation [11].

Fig. 4 also shows the computed [65] and measured [116,117,118,119,120,121] S -factors for the process ${}^3\text{He}(\alpha, \gamma){}^7\text{Be}$. Because of the larger Coulomb barrier, this reaction is more peripheral than ${}^3\text{H}(\alpha, \gamma){}^7\text{Li}$, and this is probably why its cross section depends less on V_{LSJ} . This is probably also why there is excellent agreement in the energy dependence of the cross section both with the laboratory data and with older theoretical models. The cross section normalizations of the various experiments are not completely consistent with each other, but they all show higher normalizations than do the results of our calculation, ranging from a 10% to a 100% discrepancy relative to our curve. While a 10% discrepancy is within the range allowed by the combined uncertainties of the experiments, of V_{LSJ} , and of our Monte Carlo integration, the more discrepant data sets are in clear disagreement with our result. Since the reaction is peripheral, and the branching ratio for capture into the two bound states is well reproduced, this suggests that the wave functions for both ${}^7\text{Be}$ bound states have incorrect values for their asymptotic normalizations in the $L = 1 \alpha {}^3\text{He}$ channels, and by about the same factor. Because of the discrepancies among experimental data, this reaction is a case where a microscopic model that can reliably predict the cross section normalization has the potential to shed light on the nature of the experimental difficulties and to be very useful to astrophysics. Future calculations with wave functions that are more accurate solutions for the underlying two- and three-nucleon interactions (variational or GFMC continuum states and GFMC bound states) should achieve that goal.

6.7 ${}^7\text{Be}$ weak decay

The ${}^7\text{Be}$ nucleus decays by electron (ϵ -)capture to the ground state of ${}^7\text{Li}$ and to its first-excited state at 0.478 MeV. These decays show up in the solar neutrino spectrum as two sharp lines at 0.862 and 0.384 MeV, respectively. The two ground states are both spin- $\frac{3}{2}$ states, while the ${}^7\text{Li}^*$ excited state is spin- $\frac{1}{2}$. Consequently there are both Fermi and Gamow-Teller (GT) matrix elements to ${}^7\text{Li}$, but only GT matrix elements to ${}^7\text{Li}^*$. These have been calculated using both Type I and Type II VMC wave functions as described in Sec. 5.2, in impulse approximation (IA) and with one-body relativistic, two-body meson-exchange-current, and isobar contributions [36].

The Fermi matrix element is $F = -\sqrt{2J_f + 1}$ for Type I wave functions

Table 6
Gamov-Teller matrix elements for $A=3,7$ nuclei.

	CHH		VMC(I)		VMC(II)		
	IA	Full	IA	Full	IA	Full	Expt
$^3\text{H} \rightarrow ^3\text{He}$	1.597	1.658	1.602				1.658
$^7\text{Be} \rightarrow ^7\text{Li}$			2.345(3)	2.419(5)	2.367(2)	2.433(5)	2.599
$^7\text{Be} \rightarrow ^7\text{Li}^*$			2.142(2)	2.200(3)	2.141(1)	2.205(3)	2.323

due to isospin symmetry, but is slightly less, $F = -1.999$, for Type II wave functions which include long-range Coulomb correlations. The results for GT matrix elements are shown in Table 6, where we also show the ^3H matrix elements used to fix terms beyond IA. (The $A = 7$ IA results have been updated from Ref.[36] to reflect recent improvements in the VMC wave functions.) The ^3H IA matrix elements have been calculated with both CHH and VMC wave functions with agreement to better than 0.5%. The relativistic, mesonic, and isobaric corrections total about 4% in ^3H , and 3% in ^7Be . The two types of VMC wave functions for $A = 7$ give the same results within 1%. Compared to experiment, however, the total GT matrix elements are too small by 7% for the ground state and 5% for the excited state; the corresponding half-life is calculated to be 62.3 days in IA, and 58.2 days in total, compared to the experimental 53.22 ± 0.06 days. The branching ratio to these two states is calculated to be 10.20% in IA, and 10.33% in total, compared to an experimental value of 10.44 ± 0.04 %. These calculations should be repeated with the more precise GFMC wave functions, and with an improved Hamiltonian such as AV18/IL2 that does not underbind the $A = 7$ nuclei.

7 Conclusion and prospects for the future

Recent advances in the descriptions of nuclear Hamiltonians, wave functions, and electroweak currents – as well as computer speed – may be fruitfully applied to several reaction and decay processes of interest for astrophysics. Calculations based on realistic NN interactions and currents may be relied upon for a more fundamental understanding of the nuclear systems than previous treatments. In the case of the weak captures, experimental fitting or verification of cross sections is not possible, so it is absolutely crucial to have the most fundamental theoretical understanding possible. The radiative captures are in many cases observable in the laboratory, but calculations are still necessary as tests of wave functions and currents, as guides for extrapolating laboratory data to lower energies, and (eventually) as independent sources of information on the absolute cross section.

There remains considerable opportunity for future efforts in this area. For captures producing p-shell nuclei, work is under way to develop the VMC technique for continuum states so that they can be derived directly from the

underlying NN interaction. Future improvements will include the use of the new Illinois $3N$ interactions to generate wave functions, as well as the development of methods to compute matrix elements from the (essentially exact) GFMC wave functions. More direct extraction of the asymptotic normalization coefficients from the quantum Monte Carlo wave functions may in the future prove to be very useful for direct captures.

More reactions will also be accessible in the future, partly because of improvements in algorithms and in computer speed. Ongoing work will extend theoretical calculations of the reaction $d(p, \gamma)^3\text{He}$ to higher energy. The reaction $^7\text{Be}(p, \gamma)^8\text{B}$ is an important problem in light of new laboratory data and the need to extrapolate them to solar energies. The isospin mirror process, $^7\text{Li}(n, \gamma)^8\text{Li}$ has been extensively measured [122] and will provide an interesting test of the method. Also in progress is a study of the weak decay of ^8B , which is much like the hep process in the presence of a spectator α -particle. Some longer-term prospects are $^8\text{B}(p, \gamma)^9\text{C}$ and $^4\text{He}(\alpha n, \gamma)^9\text{Be}$ reactions that may provide bridges across the $A = 5$ and $A = 8$ stability gaps in some astrophysical environments. The latter will most likely have to be treated as a neutron capture on the lowest 0^+ state of ^8Be .

As more is learned about solar neutrinos, the big bang, and other areas of nuclear astrophysics, the demand for greater precision in nuclear inputs to astrophysical calculations is increasing. Ongoing advances in theoretical treatments of reactions and decays among the light nuclei will continue to help meet this demand.

We wish to thank our collaborators J. Carlson, A. Kievsky, K. Kubodera, D.-P. Min, V.R. Pandharipande, T.-S. Park, S.C. Pieper, D.O. Riska, M. Rho, S. Rosati, and M. Viviani, for their many contributions to the present subject. The work of R.S. was supported by the U.S. DOE Contract No. DE-AC05-84ER40150, under which the Southeastern Universities Research Association (SURA) operates the Thomas Jefferson National Accelerator Facility, and that of K.M.N. and R.B.W. by the DOE, Nuclear Physics Division, under Contract No. W-31-109-ENG-38.

References

- [1] V. G. J. Stoks, et al., Phys. Rev. C 48 (1993) 792.
- [2] R. B. Wiringa, V. G. J. Stoks, R. Schiavilla, Phys. Rev. C 51 (1995) 38.
- [3] R. Machleidt, F. Sammarruca, Y. Song, Phys. Rev. C 53 (1996) R1483.
- [4] V. G. J. Stoks, et al., Phys. Rev. C 49 (1994) 2950.
- [5] S. C. Pieper, et al., Phys. Rev. C 64 (2001) 014001.
- [6] S. C. Pieper, K. Varga, R. B. Wiringa, Phys. Rev. C 66 (2002) 044310.
- [7] S. B. Dubovichenko, A. V. Dzhazairov-Kakhramanov, Phys. Atomic Nucl. 58 (1995) 579.

- [8] B. T. Kim, T. Izumoto, K. Nagatani, Phys. Rev. C 23 (1981) 33.
- [9] B. Buck, R. A. Baldock, J. A. Rubio, J. Phys. G 11 (1985) L11.
- [10] B. Buck, A. C. Merchant, J. Phys. G 14 (1988) L211.
- [11] P. Mohr, et al., Phys. Rev. C 48 (1993) 1420.
- [12] H. Walliser, et al., Phys. Rev. C 28 (1983) 57.
- [13] T. Kajino, A. Arima, Phys. Rev. Lett. 52 (1984) 739.
- [14] H. Walliser, H. Kanada, Y. C. Tang, Nucl. Phys. A419 (1984) 133.
- [15] Q. K. K. Liu, H. Kanada, Y. C. Tang, Phys. Rev. C 23 (1981) 645.
- [16] Y. Fujiwara, Y. C. Tang, Phys. Rev. C 28 (1983) 1869.
- [17] T. Kajino, Nucl. Phys. A460 (1986) 559.
- [18] T. Mertelmeier, H. M. Hoffmann, Nucl. Phys. A459 (1986) 387.
- [19] T. Altmeyer, et al., Z. Phys. A 330 (1988) 277.
- [20] A. Csótó, K. Langanke, Few-Body Systems 29 (2000) 121.
- [21] D. N. Schramm, R. V. Wagoner, Ann. Rev. Nucl. Sci. 27 (1977) 37.
- [22] H. A. Bethe, C. L. Critchfield, Phys. Rev. 54 (1938) 248.
- [23] E. G. Adelberger, et al., Rev. Mod. Phys. 70 (1998) 1265.
- [24] E. W. Kolb, M. S. Turner, *The Early Universe*, Addison-Wesley, New York, 1990.
- [25] D. N. Schramm, M. S. Turner, Rev. Mod. Phys. 70 (1998) 303.
- [26] M. S. Smith, L. H. Kawano, R. A. Malaney, Astrophys. J. Suppl. 85 (1993) 219.
- [27] R. Schiavilla, et al., Phys. Rev. C 58 (1998) 1263.
- [28] A. Nogga, H. Kamada, W. Glöckle, Phys. Rev. Lett. 85 (2000) 944.
- [29] S. A. Coon, et al., Nucl. Phys. A317 (1979) 242.
- [30] J. L. Friar, D. Hüber, U. van Kolck, Phys. Rev. C 59 (1999) 53.
- [31] J. Carlson, V. R. Pandharipande, R. B. Wiringa, Nucl. Phys. A401 (1983) 59.
- [32] B. S. Pudliner, et al., Phys. Rev. Lett. 74 (1995) 4396.
- [33] J. Carlson, R. Schiavilla, Rev. Mod. Phys. 70 (1998) 743.
- [34] J. D. Walecka, *Theoretical Nuclear and Subnuclear Physics*, Oxford University Press, New York, 1995.
- [35] L. E. Marcucci, et al., Phys. Rev. C 63 (2001) 015801.

- [36] R. Schiavilla, R. B. Wiringa, Phys. Rev. C 65 (2002) 054302.
- [37] D. O. Riska, Phys. Rep. 181 (1989) 207.
- [38] D. O. Riska, Phys. Scr. 31 (1985) 471.
- [39] R. Schiavilla, et al., Phys. Rev. C 45 (1992) 2628.
- [40] M. Viviani, R. Schiavilla, A. Kievsky, Phys. Rev. C 54 (1996) 534.
- [41] L. E. Marcucci, D. O. Riska, R. Schiavilla, Phys. Rev. C 58 (1998) 3069.
- [42] L. E. Marcucci, et al., Phys. Rev. C 66 (2003) 054003.
- [43] K. Kubodera, J. Delorme, M. Rho, Phys. Rev. Lett. 40 (1978) 755.
- [44] M. Kirchbach, D. O. Riska, K. Tsushima, Nucl. Phys. A542 (1992) 616.
- [45] T.-S. Park, et al., Phys. Rev. C 67 (2003) 055206.
- [46] A. Kievsky, M. Viviani, S. Rosati, Nucl. Phys. A551 (1993) 241.
- [47] M. Viviani, A. Kievsky, S. Rosati, Few-Body Syst. 18 (1995) 25.
- [48] A. Nogga, et al., Phys. Rev. C 67 (2003) 034004.
- [49] H. Kamada, et al., Phys. Rev. C 64 (2001) 044001.
- [50] A. Kievsky, M. Viviani, S. Rosati, Nucl. Phys. A577 (1994) 511.
- [51] A. Kievsky, M. Viviani, S. Rosati, Phys. Rev. C 52 (1995) R15.
- [52] A. Kievsky, S. Rosati, M. Viviani, Phys. Rev. Lett. 82 (1999) 3759.
- [53] A. Kievsky, C. R. Brune, M. Viviani, Phys. Lett. B 480 (2000) 250.
- [54] A. Kievsky, S. Rosati, M. Viviani, Phys. Rev. C 64 (2001) 024002.
- [55] M. Viviani, S. Rosati, A. Kievsky, Phys. Rev. Lett. 81 (1998) 1580.
- [56] M. Viviani, A. Kievsky, S. Rosati, Phys. Rev. Lett. 86 (2001) 3739.
- [57] S. C. Pieper, R. B. Wiringa, Ann. Rev. Nucl. Part. Sci. 51 (2001) 53.
- [58] A. Kievsky, L. E. Marcucci, S. Rosati, Few-Body Syst. 22 (1997) 1.
- [59] R. B. Wiringa, Phys. Rev. C 43 (1991) 1585.
- [60] N. Metropolis, et al., J. Chem. Phys. 21 (1957) 1087.
- [61] S. Cohen, D. Kurath, Nucl. Phys. 73 (1965) 1.
- [62] A. Bohr, B. R. Mottelson, Nuclear Structure Volume I, W. A. Benjamin, New York, 1969.
- [63] B. S. Pudliner, et al., Phys. Rev. C 56 (1997) 1720.
- [64] K. M. Nollett, R. B. Wiringa, R. Schiavilla, Phys. Rev. C 63 (2001) 024003.

- [65] K. M. Nollett, Phys. Rev. C 63 (2001) 054002.
- [66] R. B. Wiringa, R. A. Smith, T. L. Ainsworth, Phys. Rev. C 29 (1984) 1207.
- [67] W. Dilg, L. Koester, W. Nistler, Phys. Lett. 36B (1971) 208.
- [68] M. T. Alley, L. D. Knutson, Phys. Rev. C 48 (1993) 1901.
- [69] I. E. Lagaris, V. R. Pandharipande, Nucl. Phys. A359 (1981) 349.
- [70] K. Langanke, Nucl. Phys. A 457 (1986) 351.
- [71] V. I. Kukulin, V. N. Pomerantsev, Sov. J. Nucl. Phys. 51 (1990) 240.
- [72] V. I. Kukulin, V. N. Pomerantsev, Phys. At. Nucl. 60 (1997) 1103.
- [73] D. A. Zaikin, Nucl. Phys. A170 (1971) 584.
- [74] D. O. Riska, G. E. Brown, Phys. Lett. 38B (1972) 193.
- [75] S. F. Mughabghab, M. Divadeenam, N. E. Holden, Neutron Cross Sections from Neutron Resonance Parameters and Thermal Cross Sections, Academic Press, London, 1981.
URL <http://isotopes.lbl.gov/ngdata/sig.htm>
- [76] M. Viviani, et al., Phys. Rev. C 61 (2001) 064001.
- [77] J. W. Chen, M. J. Savage, Phys. Rev. C 60 (1999) 065205.
- [78] G. Rupak, Nucl. Phys. A678 (2000) 405.
- [79] E. E. Salpeter, Phys. Rev. 88 (1952) 547.
- [80] J. N. Bahcall, R. M. May, Astrophys. J. 152 (1969) L17.
- [81] R. J. Gould, N. Guessoum, Astrophys. J. 359 (1990) L67.
- [82] M. Kamionkowski, J. N. Bahcall, Astrophys. J. 420 (1994) 884.
- [83] M. Gari, A. H. Huffman, Astrophys. J. 178 (1972) 543.
- [84] F. Dautry, M. Rho, D. O. Riska, Nucl. Phys. A264 (1976) 507.
- [85] J. Carlson, et al., Phys. Rev. C 44 (1991) 619.
- [86] S. Ciechanowicz, E. Truhlik, Nucl. Phys. A414 (1984) 508.
- [87] J. Carlson, et al., Phys. Rev. C 42 (1990) 830.
- [88] L. E. Marcucci, et al., Phys. Rev. Lett. 84 (2000) 5959.
- [89] L. I. Schiff, Phys. Rev. 52 (1937) 242.
- [90] M. Viviani, et al., Eur. Phys. J. A 17 (2003) 483.
- [91] L. E. Marcucci, et al., Few-Body Syst. Suppl. 14 (2003) 319.
- [92] L. E. Marcucci, et al., Few-Body Syst. Suppl. 15 (2003) 87.

- [93] E. T. Jurney, P. J. Bendt, J. C. Browne, Phys. Rev. C 25 (1982) 2810.
- [94] The LUNA Collaboration, Nucl. Phys. A706 (2002) 203.
- [95] G. M. Griffiths, M. Lal, C. D. Scarfe, Can. J. Phys. 41 (1963) 724.
- [96] G. J. Schmid, et al., Phys. Rev. C 52 (1995) 1732.
- [97] G. J. Schmid, et al., Phys. Rev. Lett. 76 (1996) 3088.
- [98] R. Wervelman, et al., Nucl. Phys. A526 (1991) 265.
- [99] Y. Fukuda, et al., Phys. Rev. Lett. 86 (2001) 5651.
- [100] Y. Fukuda, et al., Phys. Rev. Lett. 82 (1999) 2430.
- [101] Y. Suzuki, contribution to Lepton-Photon Symposium 99 (1999).
URL <http://www-sk.icrr.u-tokyo.ac.jp/doc/sk/pub/index.html>
- [102] Y. Fukuda, et al., Phys. Lett. B 539 (2002) 179.
- [103] J. N. Bahcall, S. Basu, M. H. Pinsonneault, Phys. Lett. B 433 (1998) 1.
- [104] J. N. Bahcall, M. H. Pinsonneault, S. Basu, Astrophys. J. 555 (2001) 990.
- [105] R. Robertson, et al., Phys. Rev. Lett. 47 (1981) 1867.
- [106] P. Mohr, et al., Phys. Rev. C 50 (1994) 1543.
- [107] D. R. Tilley, et al., Nucl. Phys. 708 (2002) 3.
- [108] F. Cecil, J. Yan, C. Galovich, Phys. Rev. C 53 (1996) 1967.
- [109] J. Kiener, et al., Phys. Rev. C. 44 (1991) 2195.
- [110] C. Ryzhikh, R. Eramzhyan, S. Shlomo, Phys. Rev. C 51 (1995) 3240.
- [111] H. D. Holmgren, R. L. Johnston, Phys. Rev. 113 (1959) 1556.
- [112] U. Schröder, et al., Phys. Lett. B 192 (1987) 55.
- [113] G. M. Griffiths, et al., Can. J. Phys. 39 (1961) 1397.
- [114] S. Burzyński, et al., Nucl. Phys. A473 (1987) 179.
- [115] C. R. Brune, R. W. Kavanagh, C. Rolfs, Phys. Rev. C 50 (1994) 2205.
- [116] M. Hilgemeier, et al., Z. Phys A329 (1988) 243.
- [117] H. Kräwinkel, et al., Z. Phys A304 (1982) 307.
- [118] K. Nagatani, M. R. Dwarakanath, D. Ashery, Nucl. Phys. A128 (1969) 325.
- [119] P. D. Parker, R. W. Kavanagh, Phys. Rev. 131 (1963) 2578.
- [120] R. G. H. Robertson, et al., Phys. Rev. C 27 (1983) 11.
- [121] J. L. Osborne, et al., Nucl. Phys. A419 (1984) 115.
- [122] L. Trache, et al., Phys. Rev. C 67 (2003) 062801.